Scripta Materialia 204 (2021) 114141

Contents lists available at ScienceDirect

Scripta Materialia

journal homepage: www.elsevier.com/locate/scriptamat

Electric field control of the reversible magnetocaloric effect in strain-mediated $Ni_{37.5}Co_{12.5}Mn_{35}Ti_{15}$/PMN-PT composite

Kaiming Qiao[a], Shulan Zuo[d], Hu Zhang[a,*], Fengxia Hu[b,c,e,**], Ziyuan Yu[a], Fan Weng[a], Yuhang Liang[a], Houbo Zhou[b,c], Yi Long[a], Jing Wang[b,c,f], Jirong Sun[b,c,e], Tongyun Zhao[b,g], Baogen Shen[b,c,g]

[a] School of Materials Science and Engineering, University of Science and Technology Beijing, Beijing 100083, PR China
[b] Beijing National Laboratory for Condensed Matter Physics, Institute of Physics, Chinese Academy of Sciences, Beijing 100190, PR China
[c] School of Physical Sciences, University of Chinese Academy of Sciences, Beijing 100049, PR China
[d] School of Materials Science and Engineering, Beihang University, Beijing 100191, PR China
[e] Songshan Lake Materials Laboratory, Dongguan, Guangdong 523808, PR China
[f] Fujian Innovation Academy, Chinese Academy of Sciences, Fuzhou, Fujian 350108, PR China
[g] Ganjiang Innovation Academy, Chinese Academy of Sciences, Ganzhou, Jiangxi 341000, PR China

ARTICLE INFO

Article history:
Received 28 May 2021
Revised 29 June 2021
Accepted 7 July 2021
Available online 17 July 2021

Keywords:
Magnetocaloric effect
Reversibility
Electric field control magnetism
All-*d*-metal

ABSTRACT

In this study, the martensite transformation of $Ni_{37.5}Co_{12.5}Mn_{35}Ti_{15}$ ribbon was studied and regulated by the electric field-induced strain in the PMN-PT substrate. The reversible magnetocaloric effect in the $Ni_{37.5}Co_{12.5}Mn_{35}Ti_{15}$/PMN-PT composite was enhanced by manipulating transition paths under the coupling of magnetic field and electric field, which is significantly important for applications in solid-state refrigeration. With the assistance of $E = +8$ kV/cm, the reversible entropy change increased from 19.5 to 25.7 J/kgK at 294.5 K. Meanwhile, the reversible cooling temperature span was also enlarged. Hence, the reversible refrigerant capacity was enhanced from 83 to 131 J/kg, and the increase ratio reached 58%. On this basis, an active magnetic regenerating cycle facilitated by an electric field was designed. This work provides an effective method for enhancing reversible caloric effects in first-order phase transition materials via electric fields.

Solid state refrigeration technology based on the magnetocaloric effect (MCE) is rapidly developing as a potential alternative to traditional gas compressive refrigeration because of its advantages of environmentally friendly and energy-saving properties [1–5]. The application of magnetic refrigeration critically depends on the materials used. Large MCEs over a broad refrigeration temperature region are needed. The discovery of $Gd_5(Si, Ge)_4$ compounds [6] has greatly stimulated the development of the first order phase transition materials to gain large entropy change. First-order phase transition materials, such as $La(Fe, Si)_{13}$ [7,8], $MnFeP_{1-x}As_x$ [9], and Heusler alloys [10], have been widely studied as candidate materials for magnetic refrigeration in the past two decades. Particularly, recently discovered all-*d*-metal Heusler alloys $Ni_{50}Mn_{50-y}Ti_y$ and $Ni_{50-x}Co_xMn_{50-y}Ti_y$ [11–13] with first-order martensitic transformations (MTs), have produced extensive research because of their excellent mechanical stability and large caloric effects [14,15]. These types of Heusler alloys are conducive to processing into desired shapes to boost heat exchange capability, making them an ideal solid-state refrigerant. However, the poor reversibility and narrow temperature span related to intrinsic characteristics of first-order phase transition materials also exist in all-*d*-metal Heusler alloys and are longstanding obstacles for their commercialization in refrigeration. The reversibility of MCEs in first-order phase transition materials strongly depends on the width of the thermal hysteresis [16]. Therefore, it is urgent to seek an effective solution to reduce thermal hysteresis and minimize hysteresis losses. In recent years, unremitting efforts have been made to decrease thermal hysteresis in first-order phase transition materials. These efforts have included introducing chemical pressure [17], hydrostatic and uniaxial pressure [10], and reducing material size by Nano-structuring [18]. However, all of these methods concentrate on bulk samples. It has been proved that the MCE can be enhanced in $Ni_{50-x}Co_xMn_{50-y}Ti_y$ ribbons prepared by rapid solidification [19]. Therefore, it is necessary to find ways to regulate the thermal hysteresis in $Ni_{50-x}Co_xMn_{50-y}Ti_y$ ribbon samples. In recent

* Corresponding author.
** Corresponding author at: Beijing National Laboratory for Condensed Matter Physics, Institute of Physics, Chinese Academy of Sciences, Beijing 100190, PR China
E-mail addresses: zhanghu@ustb.edu.cn (H. Zhang), fxhu@iphy.ac.cn (F. Hu).

https://doi.org/10.1016/j.scriptamat.2021.114141
1359-6462/

years, great achievements have been made in the electric field control of MCEs in the laminated samples composed of a ferroelectric substrate and first-order phase transition materials [20–25]. In the present work, we propose a solution to solve the aforementioned problems (poor reversibility) through strain-mediated magnetoelectric coupling by combining $Ni_{37.5}Co_{12.5}Mn_{35}Ti_{15}$ ribbon with a ferroelectric $Pb(Mg_{1/3}Nb_{2/3})_{0.7}Ti_{0.3}O_3$ (PMN-PT) substrate. Compared with uniaxial stress or hydrostatic pressure, the electric field is more conveniently coupled with a magnetic field. It is demonstrated that the reversible MCE in $Ni_{37.5}Co_{12.5}Mn_{35}Ti_{15}$/PMN-PT composite near room temperature can be effectively enhanced through the manipulation of transition paths under the coupling of magnetic field and electric field. Moreover, the reversible refrigeration temperature span can also be broadened, thereby increasing the reversible refrigerant capacity (RC). The electric field control of reversible MCE would have great potential in the application of first-order phase transition materials in present magnetic cooling technology.

A polycrystalline ingot with the nominal composition $Ni_{37.5}Co_{12.5}Mn_{35}Ti_{15}$ was prepared by repeated melting of the high-purity raw elements in an arc furnace protected under Ar atmosphere. To compensate for the loss due to Mn evaporation during melting, an excess of 3 wt % of Mn was added before melting. The ingots were cut into small pieces, induction melted in a quartz tube and then ejected onto a copper wheel rotating with a surface velocity of 20 m/s. The resulting ribbons were ~20 μm thick and ~3.5 mm wide. The as-prepared $Ni_{37.5}Co_{12.5}Mn_{35}Ti_{15}$ ribbons were annealed at 900 °C for 1 h in a vacuumed quartz and then quenched in ice water. The ribbons were cut into pieces with a size of 5 mm × 3.5 mm and adhered by epoxy (KYOWA CC-33A) to a commercially supplied (001)-oriented PMN-PT substrate with dimensions of 5 mm × 5 mm × 0.5 mm. A gold layer was evaporated on both the top and bottom sides of the PMN-PT substrates as working electrodes. The macro- and micro- structures of the $Ni_{37.5}Co_{12.5}Mn_{35}Ti_{15}$ ribbons in the phase transition process were characterized via temperature variable X-ray diffraction (XRD, Rigaku Smart Lab) and Lorentz transmission electron microscopy (LTEM). Magnetization versus temperature (M–T) and magnetic field (M–H) curves were measured using a superconducting quantum interference device (SQUID, Quantum Design) with an *in situ* electric field applied in the thickness direction using a Keithley 6517 B.

To study the martensite transformation behavior of $Ni_{37.5}Co_{12.5}Mn_{35}Ti_{15}$ ribbons, XRD measurements were performed in the vicinity of the phase transition temperature during the cooling process. The results are shown in Fig. 1. As indicated from the pattern at 300 K, especially the presence of (200) superlattice reflections, a cubic Heusler B2 structure austenite phase with a lattice parameter of a = 5.916 Å exists without any secondary phases. Several peaks associated with martensite start to appear at 290 K and the $(220)_A$ peak intensity of the austenite phase decreases. It can also be seen that the peak intensity of martensite becomes stronger and the $(220)_A$ peak of the austenite phase gradually disappears with further decreasing temperature. At 200 K, the complete martensite phase is formed. According to careful indexation of the XRD pattern at 100 K (inset of Fig. 1(a)), the martensite in the $Ni_{37.5}Co_{12.5}Mn_{35}Ti_{15}$ ribbon exhibits a monoclinic five-layered modulated (5 M) structure with a = 4.410 Å, b = 5.410 Å, c = 21.276 Å, and β = 91.00°. This crystal structure evolution demonstrates that a typical martensitic transformation exists in the prepared ribbons. To further confirm the martensitic phase transition in the ribbon, *in situ* temperature variable LTEM was performed. Fig. 1(b) and (c) show the under-focused LTEM images of magnetic domain evolution of $Ni_{37.5}Co_{12.5}Mn_{35}Ti_{15}$ ribbon. At room temperature (297 K), the ribbon with austenite phase shows obvious ferromagnetic (FM) domain walls (Fig. 1(b)), indicating an FM austenite phase. With decreasing temperature, the FM austenite phase gradually transforms into the weak magnetic martensite phase, which is accompanied by the disappearance of magnetic domains and the appearance of acicular martensitic configurations with dark contrast (Fig. 1(c)). This also confirms the existence of the typical martensitic transformation in the prepared ribbons.

The $Ni_{37.5}Co_{12.5}Mn_{35}Ti_{15}$ ribbon with martensitic transformation was combined with a (001)-PMN-PT substrate to investigate the effect of electric field on MCEs. The M–T curves of the NiCoMnTi/PMN-PT laminate were measured under a magnetic field of 0.05 T along the in-plane [100] direction and electric fields of 0, +8, and-8 kV/cm along the out-of-plane [001] direction (see the illustration in the inset of Fig. 2). The results are shown in Fig. 2(a). It can be clearly seen that under zero electric field, the $Ni_{37.5}Co_{12.5}Mn_{35}Ti_{15}$ ribbon exhibits a phase transition from FM austenite to weak magnetic martensite upon cooling with thermal hysteresis of ~5 K. When an electric field of +8 kV/cm (or –8 kV/cm) was applied, the magnetization decreases and the transition temperature, T_t, shifts to a higher temperature, in both the heating and cooling processes, owing to the compressive stress transferred from the PMN-PT substrate [21,24]. When an electric field of +8 kV/cm (or -8 kV/cm) is applied to PMN-PT single crystal, a compressive strain along in-plane [100] and [010] direction can be generated, and then exert on the NiCoMnTi ribbon. The magnetic properties of Heusler alloys are strongly dependent on the Mn-Mn distance [26]. The electric field-induced compressive strain transferred from PMN-PT substrates would reduce the Mn-Mn distance of NiCoMnTi alloys, which enhances the antiferromagnetic interactions. Consequently, the magnetization decreases under electric fields. Similar to the effect of hydrostatic pressure [26], the compressive strain induced by an electric field would reduce the volume and the atoms become closer in the structure. This enhances orbital hybridization and bonding in the NiCoMnTi alloy [26]. Hence, more thermal energy is needed to drive the martensitic transition, leading to a shift of T_t to a higher temperature under electric fields. After removing the electric field, the magnetic state recovers and the M-T curve coincides with the initial curve, as shown in the inset of Fig. 2(a). However, the shift of T_t is about 2 K in the heating process while it is ~2.5 K in the cooling process with an electric field of +8 kV/cm. Such a difference can be ascribed to the variation with temperature of the compressive stress generated from PMN-PT. The thermal hysteresis can be reduced to 3 K by applying an electric field of +8 kV/cm in the cooling process while heating under 0 kV/cm. Except for the thermal hysteresis, the magnetic hysteresis can also be controlled by electric fields. Fig. 2(b) shows the isothermal magnetization (M–H) curves of NiCoMnTi/PMN-PT laminate at 295 K measured using the so-called loop mode [27] under electric fields of 0, +8, and –8 kV/cm. Under zero electric field, obvious metamagnetic behavior is observed, corresponding to the magnetic field-induced martensitic transformation. When an electric field is applied, the shape of the M–H curves is almost unchanged while the magnetization decreases due to the compressive strain.

To study the effect of electric field on the MCE of NiCoMnTi/PMN-PT laminate, iso-field measurements were adopted, namely, the M–T curves at 0.05 T and from 0.2 T to 5 T in 0.2 T steps, upon heating and cooling, were measured under electric fields of 0 kV/cm and +8 kV/cm. From the obtained magnetization curves, the entropy change can be determined by

$$\Delta S = [T, 0(H) \rightarrow H(0)] = \mu_0 \int_{0(H)}^{H(0)} \left(\frac{\partial M}{\partial T}\right)_H dH$$

which is the integration of the Maxwell relation of $(\partial S/\partial H)_T = \mu_0(\partial M/\partial T)_H$. The corresponding results of ΔS–T upon heating and cooling under magnetic field changes up to 5 T and electric fields of 0 kV/cm and

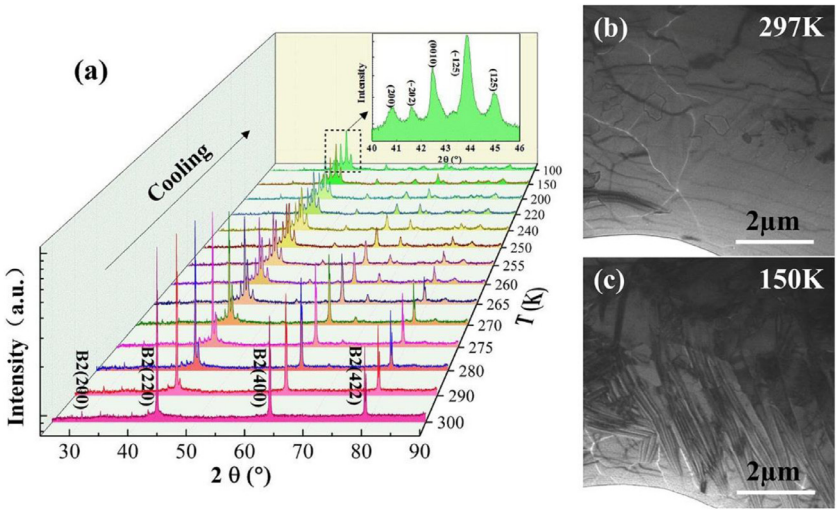

Fig. 1. (a) *In situ* XRD patterns for $Ni_{37.5}Co_{12.5}Mn_{35}Ti_{15}$ ribbon in the cooling process (from 300 to 100 K). The inset shows the partial enlarged view of the martensite XRD pattern at 100 K, where the black font indicates the 5 M martensite. (b) Room temperature and (c) low temperature (150 K) LTEM images during the cooling process of $Ni_{37.5}Co_{12.5}Mn_{35}Ti_{15}$ ribbon.

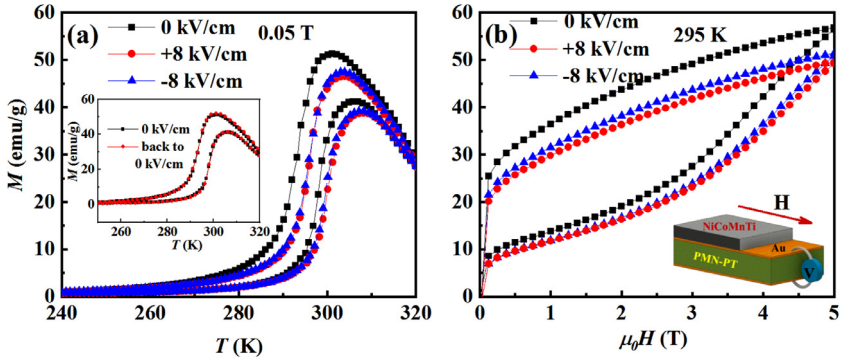

Fig. 2. (a) Temperature dependent magnetization (*M*–*T* curves) of NiCoMnTi/PMN-PT laminate with a magnetic field of 0.05 T and electric fields of 0, + 8, and –8 kV/cm. The inset shows a comparison of *M*–*T* curves in the initial state and after removing the electric field. (b) Isothermal magnetization curves under electric fields of 0, + 8, and –8 kV/cm at 295 K. The inset shows an illustration of the magnetic measurements with an *in situ* electric field.

+8 kV/cm computed from this indirect method are shown in Fig. 3(a) and (b), respectively. Clearly, the MCE increases in magnitude and the transition temperatures shift to lower values by increasing the applied magnetic field. A maximum value of ΔS ~33 J/kgK is obtained at 295.5 K under a magnetic field change of 0–5 T at 0 kV/cm during the heating process. When an electric field of +8 kV/cm is applied, the peak value of ΔS decreases to 27 J/kgK and the peak moves 2 K higher, which can be ascribed to variation of the exchange interaction induced by the compressive strain [26]. It can be clearly seen from Fig. 3(a) and (b) that the cooling temperature span determined from the full width at half maximum (FWHM) of the ΔS–*T* curves can be adjusted by the electric field. Although the FWHM both at 0 and +8 kV/cm are about 7 K, the temperature region at 0 kV/cm (292–299 K) is different from that at +8 kV/cm (294–301 K). As shown in Fig. 3(b), the cooling temperature span can be dynamically widened to 9 K, from 292 to 301 K, by tuning *E* from 0 to +8 kV/cm at temperatures larger than 296.5 K. Also, the evaluated values of *RC* for a field change of 5 T are increased from 182 to 234 J/kg by coupling the electric field of +8 kV/cm with the magnetic field, where *RC*, i.e., the energy that a refrigerant can transfer between hot and cold reservoirs, is an important parameter to evaluate the performance of MCE material. *RC* was determined from $RC = \int_{T_1}^{T_2} |\Delta S(T)| dT$, where T_1 and T_2 refer to temperatures corresponding to the FWHM in the $|\Delta S(T)|$ curves [28]. However, not all of the caloric effect in the cooling temperature span can be reversible due to thermal hysteresis. To quantify the reversible entropy change of the NiCoMnTi/PMN-PT laminate, the entropy change (ΔS) in the magnetization (demagnetization) process with the transition from martensite to austenite (from austenite to martensite) is needed. In this study, the ΔS calculated by the iso-field curves on heating (cooling) process with the transition from martensite to austenite (from austenite to martensite), is used to express the equivalent ΔS in the magnetization (demagnetization) process. This method is similar to that adopted in the quasi-direct methods [29]. It has been demonstrated that the MCE features quantified by direct, quasi-direct, and indirect methods shows good consistency in Heusler alloy [30]. Because of the inverse and mainly athermal (hysteresis rate-independent) character of the transition, the transition line crossed on magnetization (demagnetization) should be coincident with the transition line crossed on heating (cooling) [29]. Consequently, the assumption of ΔS in the magnetization (demagnetization) process calculated by the iso-field curves on heating (cooling) is reliable. Then, the reversible entropy changes are computed from the overlap between the ΔS during magnetization and demagnetization. The corresponding reversible entropy changes under 0–5 T for 0 kV/cm and on combining with E = +8 kV/cm are shown in Fig. 3(c) by the purple- and orange-shaded regions, respectively. It can be

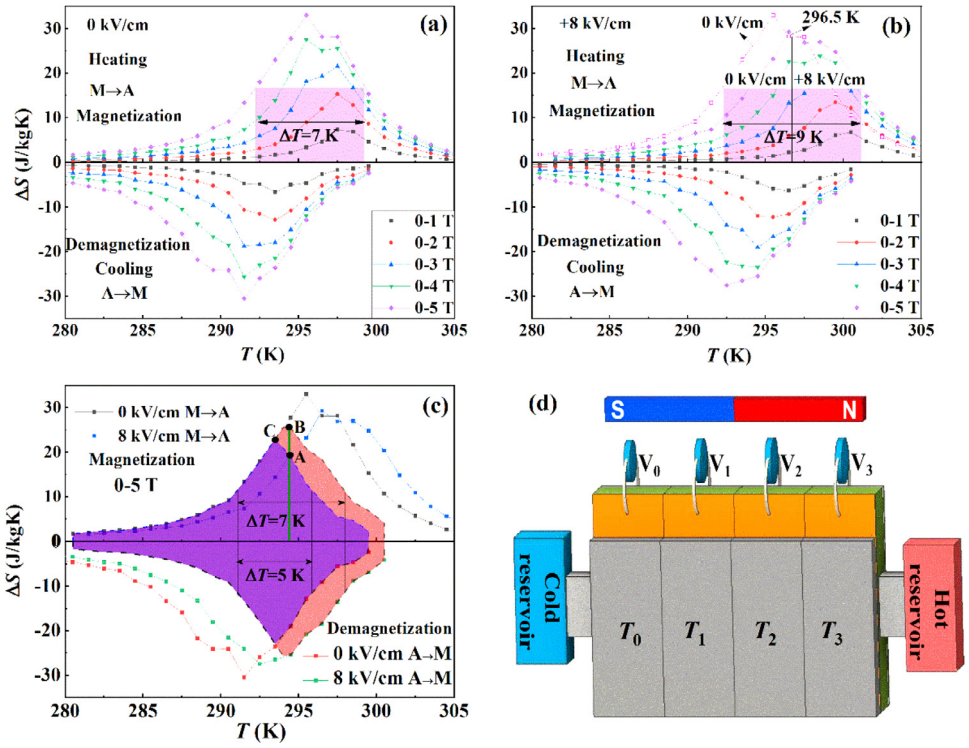

Fig. 3. Entropy change (ΔS) as a function of temperature and magnetic field for NiCoMnTi/PMN-PT laminate under electric fields of (a) 0 kV/cm and (b) +8 kV/cm during both the heating and cooling processes, where the corresponding refrigeration temperature spans in the heating process are marked by a light purple-shaded region. **(c)** Comparison of ΔS–T curves at 0–5 T under 0 and +8 kV/cm, where the corresponding reversible ΔS are marked by purple and orange shadows for conditions without E and combining with E = +8 kV/cm, respectively. (d) Schematic diagram of the active magnetic refrigerator (AMR) cycle with the assistance of electric fields.

seen that at a fixed temperature (point C in Fig. 3(c)) higher than 293.5 K, a significantly enhanced reversible entropy change can be achieved by magnetization under 0 kV/cm and then demagnetization under +8 kV/cm compared with both magnetization and demagnetization under 0 kV/cm (see the purple-shaded area). For example, at 294.5 K, the reversible ΔS is about 19.5 J/kgK (see point A in Fig. 3(c)) for the case of both magnetization and demagnetization under 0 kV/cm, while the reversible ΔS remarkably increases to 25.7 J/kgK for the case of magnetization under 0 kV/cm and then demagnetization under +8 kV/cm. Moreover, if the magnetic field was isothermally applied and removed under 0 kV/cm at temperatures lower than 293.5 K (point C), while under +8 kV/cm at the temperatures beyond 293.5 K, the working temperature window for the reversible MCE can be broadened from 5 to 7 K with the assistance of an electric field, as shown in the shaded area in Fig. 3(c). The reversible RC of the NiCoMnTi/PMN-PT laminate can be enhanced from 83 to 131 J/kg with the assistant of an electric field. Therefore, an enhancement of the reversible MCE and refrigeration temperature region has been realized by manipulating transition paths under coupled magnetic field and electric field.

For the present magnetic refrigeration prototype, the AMRs are most often used as it is considered to be an alternative refrigeration cycle with high energy efficiency compared with traditional refrigeration technology [21]. However, there is always a temperature gradient in the refrigeration process for refrigerants near the hot and cold reservoirs. Hence, each refrigerant has a different working temperature, and some of the refrigerants may not work at their optimal working temperature, leading to a reduction in the cooling performance. Based on the results above, a feasible AMR cycle with the assistance of electric fields can be designed as shown in Fig. 3(d). The optimal working temperature of each refrigerant could be tuned to its temperature by tuning the electric field and thus the reversible cooling performance could be greatly enhanced. For example, T_0 is the optimal temperature for NiCoMnTi ribbons without an electric field, while the temperature of the material bed changes from T_0 to T_3. If suitable electric fields (V_0, V_1, V_2, and V_3) were applied on different refrigerants, the optimal working temperature of each refrigerant can be tuned to be in line with the temperature of the refrigerant itself. Consequently, the reversible refrigeration performance of the AMR can be greatly enhanced with the assistance of electric fields.

In conclusion, the phase transition of $Ni_{37.5}Co_{12.5}Mn_{35}Ti_{15}$ ribbon and its regulation by the electric field-induced strain in a PMN-PT substrate were carefully studied. An enhancement of the reversible MCE and an enlargement of the refrigeration temperature span in the $Ni_{37.5}Co_{12.5}Mn_{35}Ti_{15}$/PMN-PT composite have been realized through manipulating transition paths under coupled magnetic field and electric field. With the assistance of +8 kV/cm, the reversible entropy change was increased from 19.5 to 25.7 J/kgK at 294.5 K meanwhile the cooling temperature span was enlarged from 5 to 7 K. Thus, the reversible RC was greatly enhanced from 83 to 131 J/kg, and the increase ratio reached 58%. On this basis, an AMR cycle based on electric field control of the MCE is proposed, wherein each refrigerant can operate in its optimal working temperature region with the application of suitable electric fields, thus enhancing the efficiency of the AMR. This work is important for enhancing the reversible caloric effects and enlarging the refrigeration temperature span in first-order transition materials, promoting their application in solid-state refrigeration.

Declaration of Competing Interest

The authors declare that they have no known competing financial interests or personal relationships that could have appeared to influence the work reported in this paper.

Acknowledgments

This work was supported by the National Key Research and Development Program of China (2019YFA0704900, 2020YFA0711502, 2017YFB0702704, 2018YFA0305704, 2017YFA0303601); the National Natural Sciences Foundation of China (52088101, U1832219, 51771223, 51971240, 51671022, 52001019); the China Postdoctoral Science Foundation (Grant No. 2021M690346); the State Key Lab of Advanced Metals and Materials (Grant No. 2019-Z11); the Fundamental Research Funds for the Central Universities (Grant No. FRF-GF-20–08B); and the Key Program and Strategic Priority Research Program (B) of the Chinese Academy of Sciences.

References

[1] V. Franco, J.S. Blázquez, J.J. Ipus, J.Y. Law, L.M. Moreno-Ramírez, A. Conde, Prog. Mater. Sci. 93 (2018) 112–232.
[2] K.A. GschneidnerJr, V.K. Pecharsky, A.O. Tsokol, Rep. Prog. Phys. 68 (2005) 1479–1539.
[3] X. Moya, S. Kar-Narayan, N.D. Mathur, Nat. Mater. 13 (2014) 439–450.
[4] B. Neese, B.J. Chu, S.G. Lu, Y. Wang, E. Furman, Q.M. Zhang, Science 321 (2008) 821–823.
[5] L. Manosa, A. Planes, Adv. Mater. 29 (2017) 1603607.
[6] V.K. Pecharsky, K.A. Gschneidner, Phys. Rev. Lett. 78 (1997) 4494–4497.
[7] F.X. Hu, B.G. Shen, J.R. Sun, Z.H. Cheng, G.H. Rao, X.X. Zhang, Appl. Phys. Lett. 78 (2001) 3675–3677.
[8] A. Fujita, S. Fujieda, K. Fukamichi, H. Mitamura, T. Goto, Phys. Rev. B 65 (2001) 014410.
[9] O. Tegus, E. Bruck, K.H.J. Buschow, F.R.D. Boer, Nature 415 (2002) 150–152.
[10] J. Liu, T. Gottschall, K.P. Skokov, J.D. Moore, O. Gutfleisch, Nat. Mater. 11 (2012) 620–626.
[11] Y. Shen, Z. Wei, W. Sun, Y. Zhang, E. Liu, J. Liu, Acta Mater. 188 (2020) 677–685.
[12] Z.Y. Wei, E.K. Liu, J.H. Chen, Y. Li, G.D. Liu, H.Z. Luo, X.K. Xi, H.W. Zhang, W.H. Wang, G.H. Wu, Appl. Phys. Lett. 107 (2015) 022406.
[13] Z.Y. Wei, E.K. Liu, Y. Li, X.L. Han, Z.W. Du, H.Z. Luo, G.D. Liu, X.K. Xi, H.W. Zhang, W.H. Wang, G.H. Wu, Appl. Phys. Lett. 109 (2016) 071904.
[14] Z. Wei, Y. Shen, Z. Zhang, J. Guo, B. Li, E. Liu, Z. Zhang, J. Liu, APL Mater. 8 (2020) 051101.
[15] Z.Y. Wei, W. Sun, Q. Shen, Y. Shen, Y.F. Zhang, E.K. Liu, J. Liu, Appl. Phys. Lett. 114 (2019) 101903.
[16] O. Gutfleisch, T. Gottschall, M. Fries, D. Benke, I. Radulov, K.P. Skokov, H. Wende, M. Gruner, M. Acet, P. Entel, M. Farle, Philos. Trans. R. Soc. A 374 (2016) 20150308.
[17] A. Fujita, S. Fujieda, Y. Hasegawa, K. Fukamichi, Phys. Rev. B 67 (2003) 104416.
[18] F.X. Hu, L. Chen, J. Wang, L.F. Bao, J.R. Sun, B.G. Shen, Appl. Phys. Lett. 100 (2012) 072403.
[19] H. Neves Bez, A.K. Pathak, A. Biswas, N. Zarkevich, V. Balema, Y. Mudryk, D.D. Johnson, V.K. Pecharsky, Acta Mater. 173 (2019) 225–230.
[20] R.O. Cherifi, V. Ivanovskaya, L.C. Phillips, A. Zobelli, I.C. Infante, E. Jacquet, V. Garcia, S. Fusil, P.R. Briddon, N. Guiblin, A. Mougin, A.A. Unal, F. Kronast, S. Valencia, B. Dkhil, A. Barthelemy, M. Bibes, Nat. Mater. 13 (2014) 345–351.
[21] Y.Y. Gong, D.H. Wang, Q.Q. Cao, E.K. Liu, J. Liu, Y.W. Du, Adv. Mater. 27 (2015) 801–805.
[22] Q.B. Hu, J. Li, C.C. Wang, Z.J. Zhou, Q.Q. Cao, T.J. Zhou, D.H. Wang, Y.W. Du, Appl. Phys. Lett. 110 (2017) 222408.
[23] K. Qiao, F. Hu, Y. Liu, J. Li, H. Kuang, H. Zhang, W. Liang, J. Wang, J. Sun, B. Shen, Nano Energy 59 (2019) 285–294.
[24] K. Qiao, J. Wang, F. Hu, J. Li, C. Zhang, Y. Liu, Z. Yu, Y. Gao, J. Su, F. Shen, H. Zhou, X. Bai, J. Wang, V. Franco, J. Sun, B. Shen, Acta Mater. 191 (2020) 51–59.
[25] Y. Liu, L.C. Phillips, R. Mattana, M. Bibes, A. Barthelemy, B. Dkhil, Nat. Commun. 7 (2016) 11614.
[26] S. Esakki Muthu, N.V. Rama Rao, M. Manivel Raja, S. Arumugam, K. Matsubayasi, Y. Uwatoko, J. Appl. Phys. 110 (2011) 083902.
[27] L. Caron, Z.Q. Ou, T.T. Nguyen, D.T. Cam Thanh, O. Tegus, E. Brück, J. Magn. Magn. Mater. 321 (2009) 3559–3566.
[28] K.A. Gschneidner Jr, V.K. Pecharsky, A.O. Pecharsky, C.B. Zimm, Mater. Sci. Forum 315–317 (1999) 69–76.
[29] P. Lloveras, T. Samanta, M. Barrio, I. Dubenko, N. Ali, J.L. Tamarit, S. Stadler, APL Mater. 7 (2019) 061106.
[30] E. Stern-Taulats, P.O. Castillo-Villa, L. Mañosa, C. Frontera, S. Pramanick, S. Majumdar, A. Planes, J. Appl. Phys. 115 (2014) 173907.